ACS NANO
Cite This: ACS Nano XXXX, XXX, XXX−XXX
www.acsnano.org

ARTICLE

# An Ultra-Low-Friction Triboelectric−Electromagnetic Hybrid Nanogenerator for Rotation Energy Harvesting and Self-Powered Wind Speed Sensor

Peihong Wang,[†,‡,⊥] Lun Pan,[‡,§,⊥] Jiyu Wang,[‡] Minyi Xu,[‡] Guozhang Dai,[‡] Haiyang Zou,[‡] Kai Dong,[‡] and Zhong Lin Wang*[,‡,∥]

[†]School of Physics and Materials Science, Anhui University, Hefei, Anhui 230601, China
[‡]School of Materials Science and Engineering, Georgia Institute of Technology, Atlanta, Georgia 30332-0245, United States
[§]Key Laboratory for Green Chemical Technology of the Ministry of Education, School of Chemical Engineering and Technology, Tianjin University, Tianjin 300072, China
[∥]Beijing Institute of Nanoenergy and Nanosystems, Chinese Academy of Sciences, Beijing 100083, China

Supporting Information

**ABSTRACT:** **Triboelectric nanogenerators (TENGs) are attracting more and more attention since they can convert various mechanical energies into electric energy. However, in traditional TENGs for harvesting rotation energy, most of the contacts between two triboelectric materials are rigid-to-rigid contact with very large friction force, which limits their practical application. Here, we report an ultra-low-friction triboelectric−electromagnetic hybrid nanogenerator (NG). A freestanding mode TENG and a rotating electromagnetic generator (EMG) are integrated together to realize the complementary individual merits. The very soft and elastic contact between the two triboelectric materials in the TENG results into very small friction force. The influences of the type and the dimensions of the dielectric material on the performance of the TENG are studied systematically from theory to experiments. The results indicate that the open-circuit voltage and the transfer charge of the TENG increase with the rotation speed, which is very different from a traditional rotary TENG and is due to the increase of the contact area. The optimized TENG has a maximal load voltage of 65 V and maximal load power per unit mass of 438.9 mW/kg under a speed rotation of 1000 rpm, while the EMG has a maximal load voltage of 7 V and maximal load power density of 181 mW/kg. This demonstration shows that the hybrid NG can power a humidity/temperature sensor by converting wind energy into electric energy when the wind speed is 5.7 m/s. Meanwhile, it can be used as a self-powered wind speed sensor to detect wind speed as low as 3.5 m/s.**

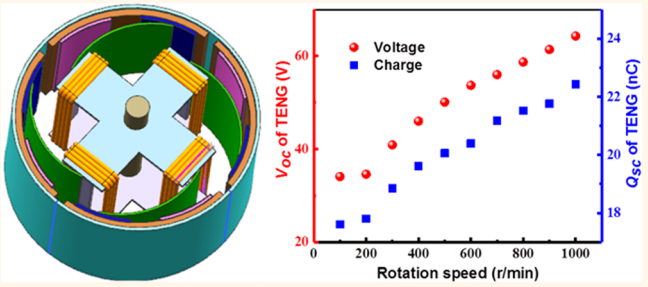


**KEYWORDS:** *triboelectric nanogenerator, electromagnetic generator, hybrid nanogenerator, ultra-low-friction, rotating energy, wind energy, wind speed sensor*

With the fast development of microelectronics technology and microelectromechanical systems (MEMS), more and more microsensors, actuators, and MEMS devices are being widely used in various fields, such as wireless sensor networks, the Internet of Everything, wearable electronics, and electric skins.[1−5] Meanwhile, their demand for a power source is becoming more and more stringent. Traditional power sources, such as batteries and electric cables, cannot meet the requirements of these microdevices, such as wireless, portable, long life, environmentally friendly, and even implantable. As a very promising alternative to traditional power sources, the energy-harvesting technique,[6−10] which can convert various energies in the environment into electric energy, has attracted more and more attention in the past decades. Triboelectric nanogenerators (TENGs),[11−14] whose working mechanism is from the triboelectrification effect and electrostatic induction, have been considered as one of the most effective energy conversion

Received: June 19, 2018
Accepted: September 11, 2018
Published: September 11, 2018






DOI: 10.1021/acsnano.8b04654
ACS Nano XXXX, XXX, XXX−XXX

techniques. TENGs can convert almost all kinds of mechanical energies into electric power,[15−26] since they have many advantages such as light weight, high output voltage, simple fabrication, and excellent reliability. However, the output current of TENGs is very low.[27] On the other hand, an electromagnetic generator (EMG) also can convert various mechanical energies into electric energy but has the disadvantage of low output voltage. Therefore, many works hybridize EMG and TENG together and try to reveal their advantages and complementary features of harvesting mechanical energy and self-powered sensing.[28,29] Zhong *et al.* reported a hybrid nanogeneraotor that can simultaneously harvest biomechanical energy from rotation, then drive a commercial globe light to work.[30] Guo *et al.* presented a waterproof hybrid nanogeneraotor to scavenge wind energy and water-flow energy in harsh environments.[31] In addition, Wen *et al.* proposed a hybrid nanogeneraotor that can work under rotation mode or fluctuation mode, as its design is very unique.[32] Although these rotating hybrid NGs have high output performance, the rotation is driven by a large external force from an electric motor, water, or wind with high flow speed.[17,30,33−36] If the driven force is small, these hybrid NGs cannot work since the friction between the two triboelectric materials is too high. Therefore, a more suitable design of a hybrid NG to obtain low friction force and high output performance is required.

Herein, we report an ultra-low-friction triboelectric−electromagnetic hybrid nanogenerator (ULFHG) for harvesting rotation energy. It consists of a rotary-blade-based TENG and a rotary EMG. The TENG works on the sliding freestanding triboelectric-layer mode.[37,38] What is more, the contact between the two triboelectric materials is very soft due to the high flexibility of the dielectric film,[20,39] which is very different from traditional rigid−rigid contact. Therefore, the TENG can work under very low external driven force. The effect of the structure parameters of every part of the TENG on its performance is investigated in detail from theory and experiment in this work. The demonstration shows that the ULFHG not only can scavenge various rotation energies but also can detect wind speed. This ULFHG will have great potential applications in scavenging wind energy with very low wind speed or very weak rotating energy and detecting very weak wind.

## RESULTS AND DISCUSSION

**Structure and Working Mechanism.** The device schematic of our hybrid NG is shown in Figure 1a, which mainly includes a rotator and a cylindrical stator. The rotator is composed of a shaft and a cross-shaped vertical structure with four groups of handmade coils and four elastic blades made of flexible triboelectric materials (*i.e.*, polymer thin film). The coil's area and the number of turns of one coil are about 7.5 $cm^2$ and 100, respectively, and these four coils are connected in series in order to increase the output voltage. The length of the polymer thin film along the shaft's direction is 4 cm, and the length along another direction will be optimized in the following. The stator is a tube structure with two covers on its top and bottom sides (to stabilize the shaft of the rotator). Four pieces of arc-shaped magnets are attached on the inner wall of the stator, and the poles of two adjacent magnets are opposite. The inner diameter and outer diameter of the four-magnet cylinder are 5.5 and 6.5 cm, respectively, while the height of the magnetic cylinder is 4 cm. Meanwhile, eight

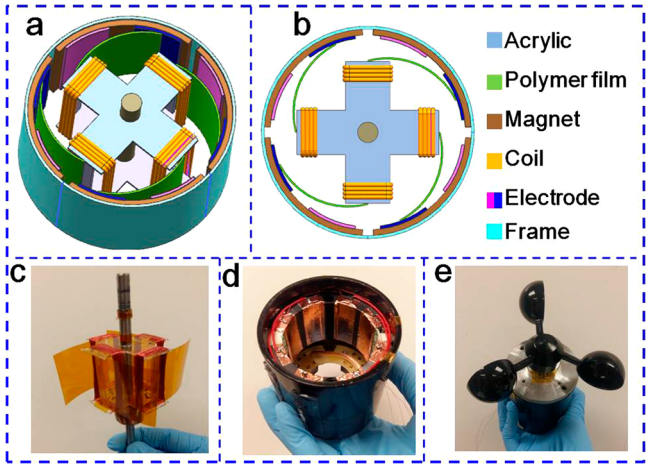


**Figure 1. Device schematic of the hybrid nanogeneraotor. (a, b) Schematic illustration of the hybrid nanogeneraotor. Optical photographs of (c) the rotator with handmade coils and polymer thin films (Kapton), (d) the stator with separated Cu electrodes and magnets, and (e) the assembled hybrid NG with wind cups.**

pieces of copper (Cu) foils are attached on the magnets as conductive electrodes with the same gap between each other. The length and the width of one Cu electrode are 4 and 1.5 cm, respectively. In this device, the magnets and the coils form an EMG, while the flexible polymer thin films and the Cu electrodes form a sliding-freestanding triboelectric nanogenerator (SF-TENG). Eight electrodes are divided into two groups with two adjacent electrodes in different groups. Other relative fabrication information is in the Experimental Section.

The working principles of the SF-TENG and the rotating EMG in this hybrid NG are illustrated in Figure 2a,b, respectively. It can be seen from Figure 2a (I) that the polymer film contacts the Electrode-1 at the initial state. According to the contact triboelectrification effect, the electrons in Electrode-1 are injected into the polymer film because polymer film is more triboelectrically negative than metal.[29] Therefore, equal amounts of charges with different polarities are accumulated on the two contact surfaces (Figure 2a (I)). When the polymer film rotates to the left and then contacts Electrode-2, the electrons in Electrode-2 will flow into Electrode-1 through the external circuit, which results in the gradual accumulation of positive charges on the surface of Electrode-2 (Figure 2a (II)). As shown in Figure 22a (III), when the polymer film is completely separated from Electrode-1, all positive charges on Electrode-1 are neutralized by electrons from Electrode-2. Subsequently as shown in Figure 2a (IV), the polymer film contacts Electrode-1 again and the electrons in Electrode-1 flow into Electrode-2. Accordingly, the direction of the current in the external circuit changed. When the polymer film is completely separated from Electrode-2 (Figure 2a (I)), a new half working cycle starts.

The working operation of the EMG is illustrated in Figure 2b. At the initial state as shown in Figure 2b (I), the coil is closest to the magnet and the magnetic flux linkage through the coil is largest. When the coil starts to rotate, the coil generates induced current due to the change of the magnetic flux linkage. As indicated in Figure 2b (II), the direction of the induced current in the adjacent coil is opposite because the adjacent magnet has opposite magnetic polarity. Subsequently, the magnetic flux linkage through the coil continues to decrease until the coil is closest to the next magnet, and the


DOI: 10.1021/acsnano.8b04654
*ACS Nano* XXXX, XXX, XXX−XXX

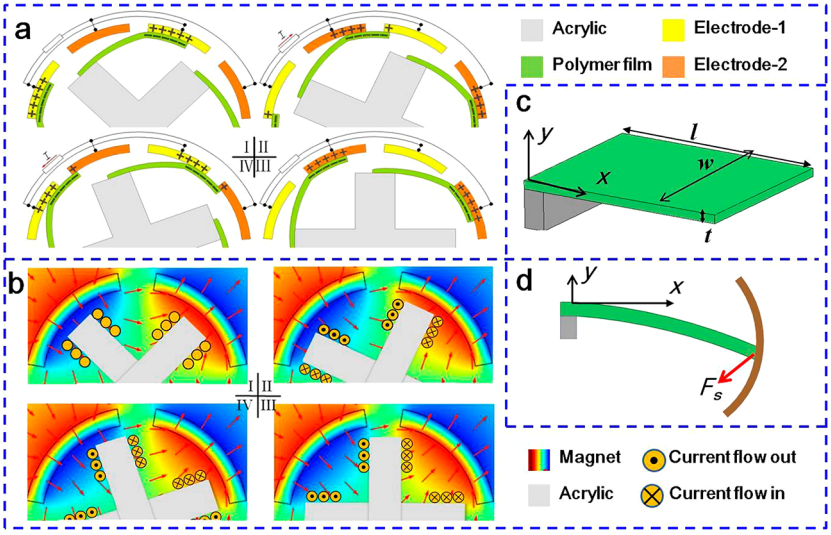


**Figure 2. Schematic working principle of (a) the SF-TENG and (b) the EMG at four states (from I to IV) in a half-device. (c) Schematic of a cantilever beam without load and (d) deformation of the blade under the supporting force from the stator when the blade is stationary.**

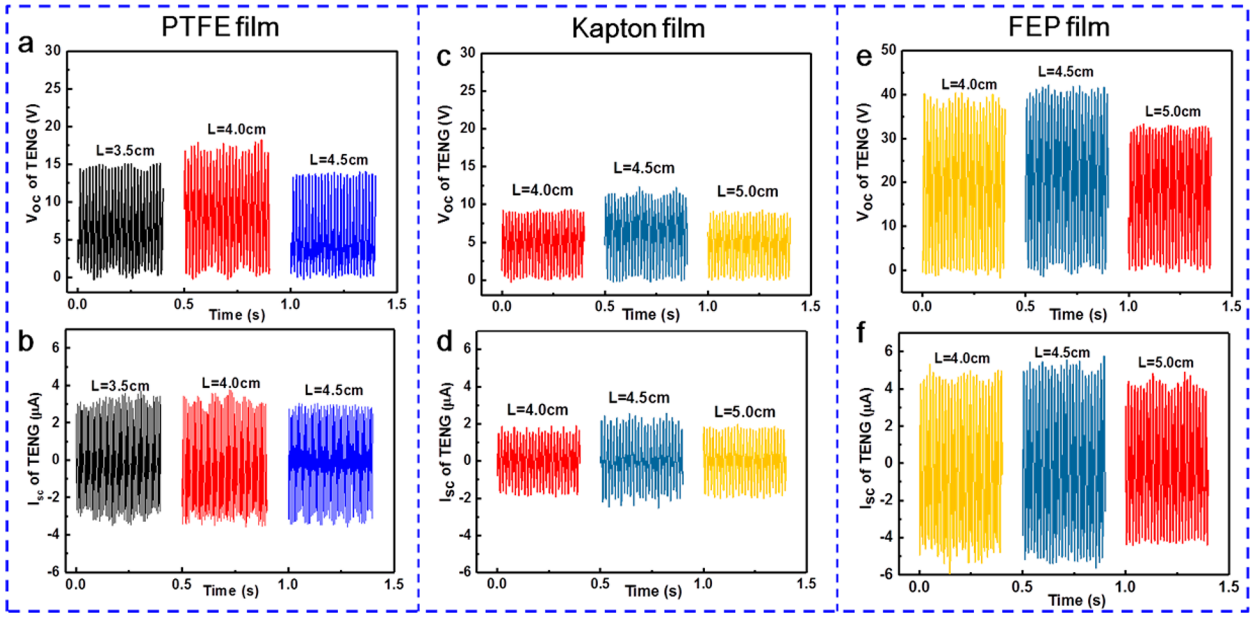


**Figure 3. Output characterization of the SF-TENG made of different triboelectric materials with different length: (a, b) PTFE film; (c, d) Kapton film; (e, f) FEP film.**

induced current's direction is constant (Figure 2b (III) and (IV)). After that, half of the working cycle is finished.

**Theoretical Analysis.** For an EMG, its open-circuit voltage ($V_{oc}$) and short-circuit current ($I_{sc}$) can be represented as[28,31]

$$V_{oc}^{EMG} = -N\frac{d\phi}{dt} \quad (1)$$

$$I_{sc}^{EMG} = \frac{V_{oc}^{EM}}{R_{coil}} \quad (2)$$

where $N$ is the turn number of the coil, $\phi$ is the magnetic flux linkage, and $R_{coil}$ is the coil's resistance.

For a rotational TENG, the $V_{oc}$ and the transfer charge ($Q_{sc}$) under short-circuit conditions can be represented as[31,37]

$$V_{oc}^{TENG} = \frac{\sigma S}{C} \quad (3)$$

$$Q_{sc}^{TENG} = \int I_{sc}\, dt \quad (4)$$

where $\sigma$ is the transfer charge density, $S$ is the contact area between two triboelectric materials, and $C$ is the capacitance.

When the blade is free, it can be considered as a cantilever beam, as shown in Figure 2c, and its spring constant $k$ is[40]

$$k = \frac{Ewt^3}{4l^3} \quad (5)$$

where $t$ is the thickness, $w$ is the width and $l$ is the thickness of the cantilever, and $E$ is the Young's modulus of the polymer film. The cantilever can deform when a concentrated load $F$ along the $y$-axis is applied on the free end of the cantilever, as



DOI: 10.1021/acsnano.8b04654
ACS Nano XXXX, XXX, XXX−XXX

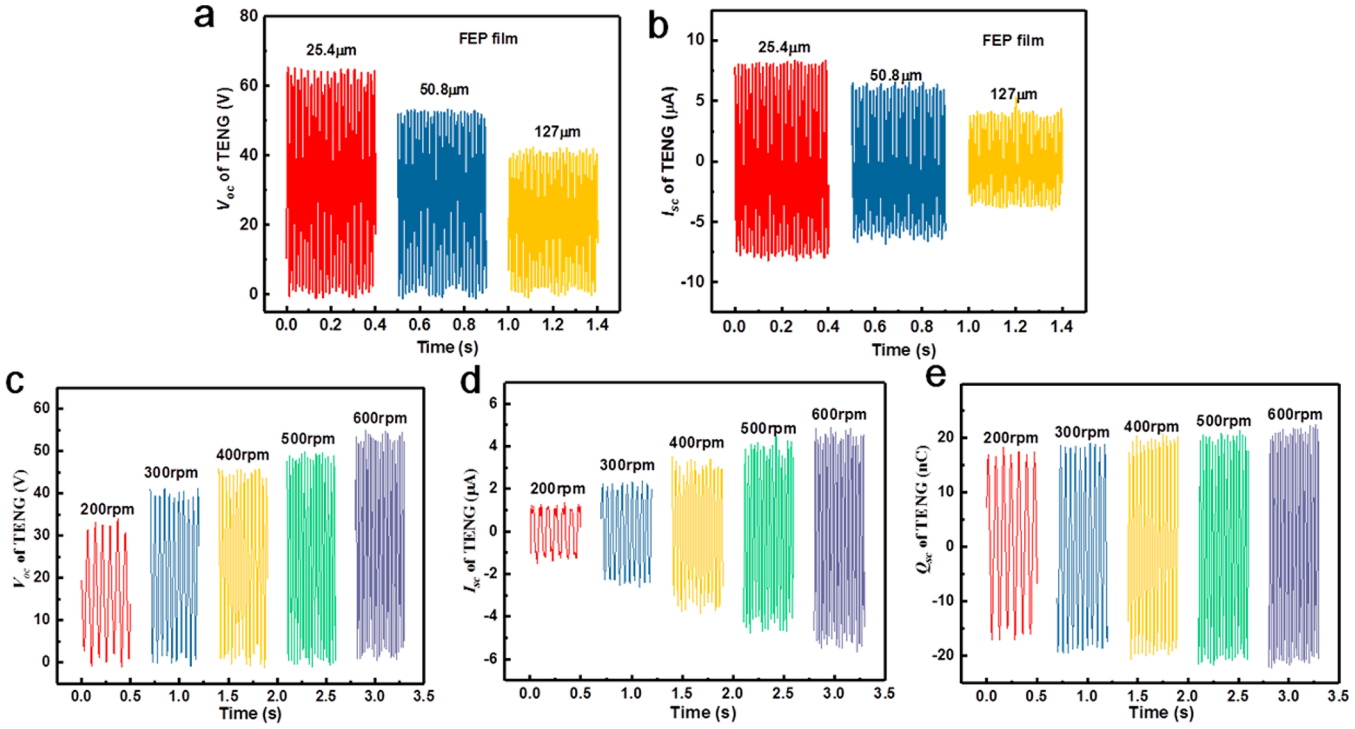


**Figure 4. Output performance of the tirboelectric nanogenerator with FEP film. (a) $V_{oc}$ *versus* time and (b) $I_{sc}$ *versus* time under different FEP film thicknesses; (c) $V_{oc}$ *versus* time, (d) $I_{sc}$ *versus* time, and (e) $Q_{sc}$ *versus* time under different rotation speeds.**

indicated in Supplementary Figure 1. The cantilever's deformation is[40]

$$y(x) = \frac{-2F}{Ewt^3}(3x^2l - x^2) \tag{6}$$

where $x$ is the coordinate of every point of the cantilever on the $X$-axis. When the blade contacts the stator and deforms with no rotation as shown in Figure 2d, a concentrated load is supplied by the inner side of the stator and is always part of the supporting force ($F_s$) from the stator. When the blades are moving in a circular motion at a fixed speed, the centripetal force ($F_c$) applied on the blade is

$$F_c = m\omega^2 r \tag{7}$$

where $\omega$ is the angular velocity, $m$ is the mass, and $r$ is the radius. The centripetal force of the blade's part contacting the stator is supplied by the supporting force $F_s$; meanwhile, the centripetal force of the blade's part without contacting the stator is supplied by the elastic force of the blade. With the increase of rotation speed, when the elastic force cannot supply sufficient centripetal force, the blade has to contact the stator so that the supporting force can supply centripetal force. Therefore, the contact area between the blade and the stator increases with the rotation speed, which will be proved by the following experiments. On the other hand, the elastic force is determined by the spring constant. Therefore, the optimization of the triboelectric material's type, the dimension of the blade, and the rotation speed is essential and was conducted in the following experiments.

**Output Characterization.** First, the effect of the triboelectric material's type and the length of the blade on the output performance of the TENG was investigated systematically. In this experiment, polytetrafluoroethylene (PTFE), fluorinated ethylene propylene (FEP), and Kapton thin films were used as the blade's materials. They possess the same thickness of 127 $\mu$m, same width of 4 cm, and different length from 3.5 to 5 cm. A motor was used to supply the rotation motion with a speed of 1000 rpm. It can be noted from Figure 3 that both the $V_{oc}$ and the $I_{sc}$ of the TENG have a maximum during increasing the length of the blade for each triboelectric material. Meanwhile, the length of the blade corresponding to maximal output is different for different triboelectric materials. If the blade is too long, the blade will contact two electrodes simultaneously at any time, which will make the output voltage smaller. On the other hand, we can find from Figure 3 that the TENG with a 4.5 cm long FEP blade has the highest $V_{oc}$ of 42 V and $I_{sc}$ of 5.1 $\mu$A. Since the Young's modulus of FEP is smaller than that of PTFE and Kapton, the smaller spring constant of the blade made of FEP film results in a bigger contact area. Therefore, the TENG made of FEP film has the highest output. As a result, FEP film with a length of 4.5 cm is used as the blade material in the following experiments.

Then, the influence of the FEP film's thickness and the rotation speed on the output performance of the TENG was studied, and the results are shown in Figure 4. Three types of FEP blades with different thicknesses of 127, 50.8, and 25.4 $\mu$m are applied, and the rotation speed is fixed as 1000 rpm (Figure 4a,b). The $V_{oc}$ of the TENG increases from 40.9 V to 64.3 V and the $I_{sc}$ increases from 5.5 $\mu$A to 8.24 $\mu$A when decreasing the thickness of the FEP film from 127 $\mu$m to 25.4 $\mu$m. According to eq 5, the decrease of the FEP film thickness results in the decrease of the spring constant, which leads to the decrease of the elastic force. Then the contact area between the FEP film and Cu electrodes has to increase in order to supply sufficient centripetal force. Therefore, the $V_{oc}$ of the TENG will increase with the enlarged contact area according to eq 3. The increase of the contact area results in the increase of transfer charge $Q$ in the same period. According to the equation $I_{sc} = dQ/dt$, the $I_{sc}$ of the TENG increases with


DOI: 10.1021/acsnano.8b04654
ACS Nano XXXX, XXX, XXX−XXX

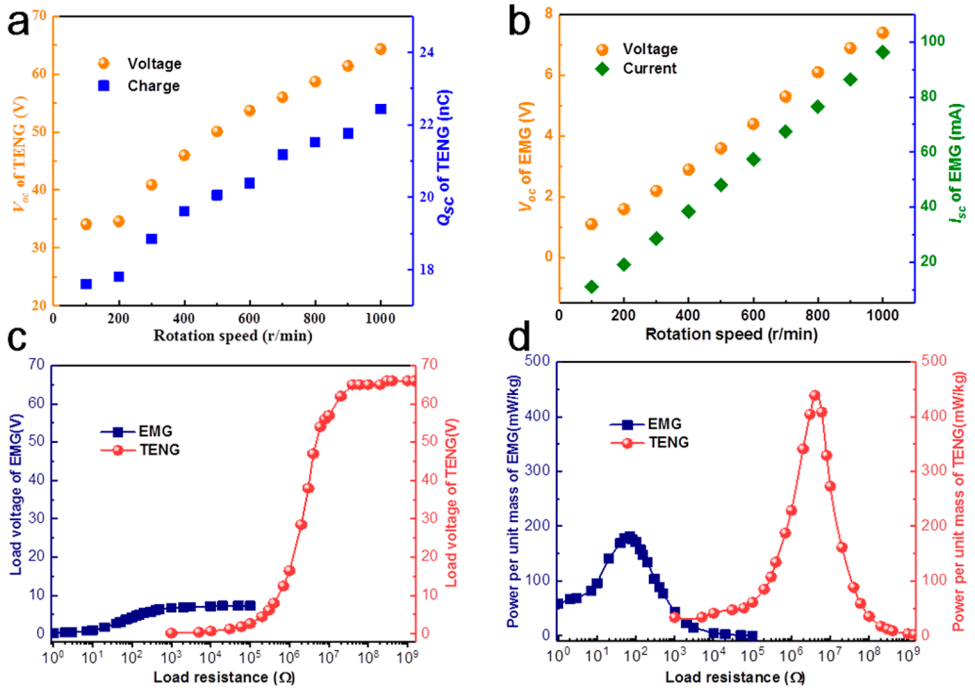


**Figure 5. Output performance of the hybrid nanogenerator under different rotation speeds and load resistances. (a) $V_{oc}$ and $Q_{sc}$ of the TENG *versus* rotation speed. (b) $V_{oc}$ and $I_{sc}$ of an EMG *versus* rotation speed. $V_{oc}$ (c) and output power density (d) of an EMG and TENG *versus* load resistance under a rotation velocity of 1000 rpm.**

decreasing the thickness of the FEP film, as shown in Figure 4b. Based on the above results, the FEP film with a 25.4 $\mu$m thickness is used in the following experiments.

Figure 4c–e show the measured results of $V_{oc}$, $I_{sc}$, and $Q_{sc}$ of the triboelectric nanogenerator under several different rotation speeds. It is clear in Figure 4c that the $V_{oc}$ increases with the rotation speed gradually, which is obviously different from traditional rotary TENGs. In traditional rotary TENGs,[17,30,33−36] the contact area and the contact degree of two triboelectric materials are unchangeable. Therefore, the $V_{oc}$ keeps constant regardless of the rotation speed according to eq 3. However, in our designed TENG, the situation is very different. The experimental setup in Supplementary Figure 2 was used to measure the contact area between the blade and the stator under different speeds, and the results are in Supplementary Figure 3. This figure shows that the contact area increases gradually when the rotation speed increases from 100 rpm to 1000 rpm According to eq 3, the $V_{oc}$ of the TENG increases with the contact area and so increases with the rotation speed as shown in Figure 4c. Figure 4d indicates that the $I_{sc}$ of the TENG also increases with the rotation speed, which is the same as a traditional rotary TENG and is due to the gradually promoted charge-transfer rate. Figure 4e shows that the $Q_{sc}$ increases with the rotation speed, which is attributed to the increase in the contact area, too.

The electrical performance of the individual TENG parts and the individual EMG parts *versus* the rotation speed was further investigated. As shown in Figure 5a, the $V_{oc}$ and the $Q_{sc}$ of the TENG respectively increase from 34.1 V to 64.3 V and 17.6 nC to 22.4 nC gradually when the rotation speed rises from 100 rpm to 1000 rpm. It is clear that the $V_{oc}$ of the TENG increases slowly at first and then increases greatly. Under low rotation speed, since the elastic force can supply sufficient centripetal force for the blade, the contact area increases little, and so the $V_{oc}$ of the TENG remains almost constant. During the increase of the rotation speed, when the elastic force in the blade cannot supply sufficient centripetal force for the blade, the blade has to contact the stator gradually so that the supporting force from the stator can supply centripetal force. Therefore, the contact area increases greatly, which results in the great increase of the $V_{oc}$ under high speed according to eq 3. By comparing Supplementary Figure 4 with Figure 5a, we can find that the change trend of the contact area is very similar to that of the $V_{oc}$ of the TENG, which proves the correctness of the $V_{oc}$ of the TENG in Figure 5a. On the other hand, the $Q_{sc}$ of the TENG has a similar change trend to the $V_{oc}$ of the TENG, as shown in Figure 5a, which is attributed to the linear relationship between the $Q_{sc}$ and the $V_{oc}$ of the TENG. Figure 5b shows that there is a linear relationship between the $V_{oc}$ and the $I_{sc}$ of the EMG and the rotation speed, which is consistent with eqs 1 and 2. The load voltage and the load power per unit mass of the TENG and that of the EMG under different resistances are compared in Figure 5c,d. Since the EMG has a very low internal resistance, its load voltage reaches a maximum of about 7 V very fast during the progress of increasing the load resistance (Figure 5c). By contrast, the load voltage of the TENG reaches its maximum of about 65 V when the external resistance is about 50 MΩ, as indicated in Figure 5c. The load power per unit mass of the TENG and that of the EMG can be calculated by using $P = V^2/(m \times R)$ and are shown in Figure 5d. The maximal power per unit mass of the EMG is 181 mW/kg when the resistance is about 80 Ω. Meanwhile, the maximal power per unit mass of the TENG is 438.9 mW/kg when the external load resistance is about 40 MΩ. Since the EMG part in our device has four big magnets but the TENG part only has several light FEP films and thin Cu electrodes, the maximal power per unit mass of the TENG is larger than that of the EMG even under high rotation speed. Therefore, the TENG has a larger output power density than the EMG in this hybrid NG.



DOI: 10.1021/acsnano.8b04654
*ACS Nano* XXXX, XXX, XXX−XXX

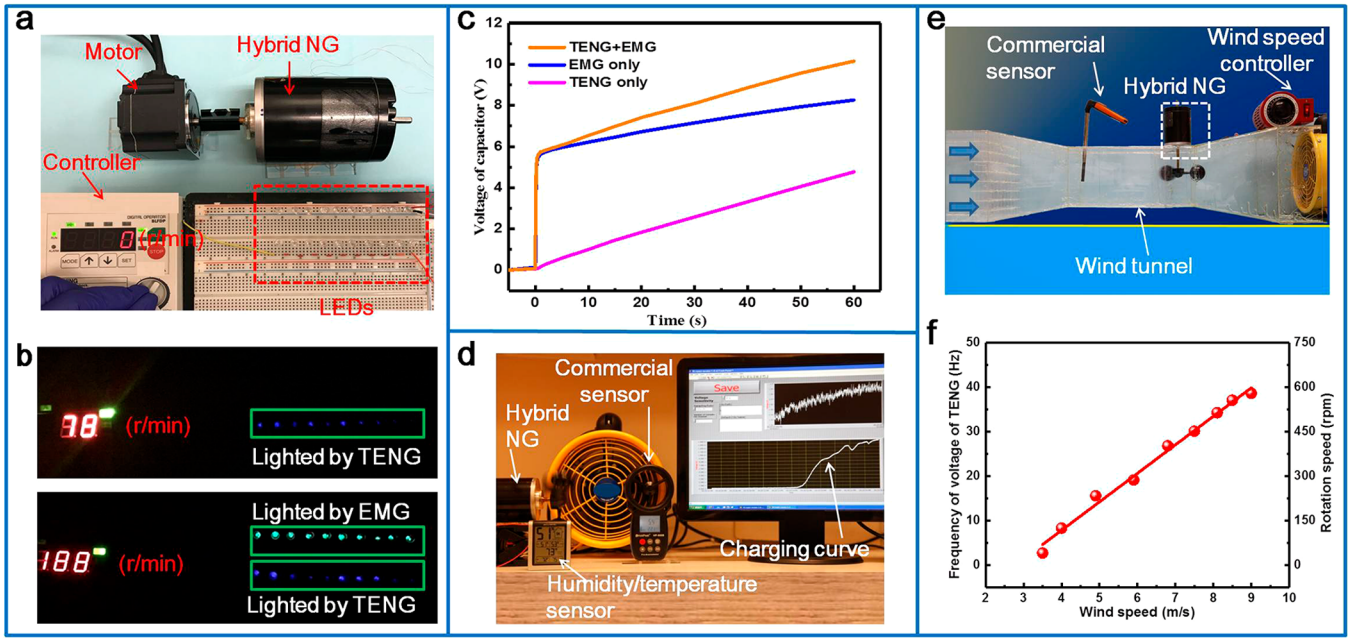


**Figure 6. Demonstration of the ultra-low-friction hybrid NG for energy scavenging and self-powered wind speed sensing. (a) Photograph of the setup for harvesting rotation energy. (b) Pictures of 10 LEDs lighted by a TENG or EMG and corresponding rotation speed. (c) Charging curve of the TENG, EMG, and the hybrid NG when the capacitor is 100 $\mu$F. (d) Photograph of a humidity and temperature sensor powered by the hybrid NG by scavenging wind energy. (e) Photograph of the setup for measuring the wind speed by using the hybrid NG. (f) Relationship between the frequency of voltage, the rotation speed, and the wind speed.**

**Demonstration.** In order to demonstrate this nanogenerator's capability to harvest rotation energy, commercial light-emitting diodes (LEDs) were directly connected with it without using any regulation units (Figure 6a). Ten green LEDs in parallel are connected with the EMG part and 10 blue LEDs in series are connected with the TENG part. As indicated in Figure6b, the blue LEDs are lighted totally by the TENG when the rotation speed arrives at 78 rpm; however, the EMG lights the green LEDs until the rotation speed reaches 188 rpm. Therefore, the TENG already has the ability to drive small electric devices under a very low working frequency (~1 Hz). In contrast, the EMG has the capability at high rotation speed or operation frequency (>3 Hz). With a further increase in rotation speed, the LEDs powered by the EMG start to have a higher brightness than the LEDs powered by the TENG. Therefore, the TENG part and the EMG part have very good complementarity on supplying energy in a large frequency range. The detailed experiment is displayed in Movie S1.

Then, the charging capability of this hybrid NG was investigated and compared with that of an individual TENG or individual EMG. A capacitor of 100 $\mu$F is used, and the rotation speed is 1000 rpm in this experiment. As exhibited in Figure 6c, the charging speed of the TENG is faster than the charging speed of the EMG, although the charged voltage of the EMG is larger than that of the TENG at the beginning of the charging process. This means that the capacitor's voltage from the TENG will be larger than that from the EMG after a longer time. Moreover, it can be found that in 60 s the voltage of the capacitor charged by the TENG, EMG, and hybrid NG reaches 4.7, 8.3, and 10.2 V, respectively. In addition, the charging time of the hybrid NG for a given voltage is the shortest. Therefore, the hybrid NG has the best charging performance. The charging curve of a 10 $\mu$F capacitor shown in Supplementary Figure 5 also proves the correctness of the above conclusion.

Furthermore, the capability of this hybrid NG for harvesting wind energy and powering a small electric device is demonstrated in Figure 6d. The hybrid NG is driven by the wind from a wind turbine, and the wind speed is about 5.7 m/s. A 10 $\mu$F capacitor is used to store the electric energy and then power a humidity and temperature sensor. The corresponding working circuit is given in Supplementary Figure 6. It can be found that the sensor is successfully lit up after about 8 s of charging. What is more, the sensor can work continuously after it is turned on. The detailed experiment is displayed in Movie S2. It shows that this hybrid NG will have potential applications in wind energy harvesting, flow energy harvesting, and so on.

In addition to energy harvesting, this ultra-low-friction TENG can also be used to detect wind speed. The photograph of the whole testing setup is given in Figure 6e. A homemade wind tunnel was utilized to generate continuous wind to drive the TENG. A commercial hot-wire anemometer was used to measure the wind speed. The output performance of the TENG greatly depends on the environment conditions such as the humidity and temperature.[14,20] However, the frequency of output signal of the TENG depends only on the wind speed regardless of environment conditions.[20,39] Therefore, this work uses the frequency of voltage of the TENG to detect the wind speed. As shown in Figure 6f, with the wind speed increasing from 3.5 m/s to 9.0 m/s, the frequency of the voltage increases linearly from 2.68 Hz to 38.6 Hz. Since the rotation speed ($V$) is linear with the frequency of voltage ($f$) ($V = f/4 \times 60$), the rotation speed *versus* wind speed is the same as the frequency of voltage *versus* wind speed, as indicated in Figure 6f. The lowest wind speed that the TENG can detect is 3.5 m/s smaller than other TENG-based wind speed sensors,[41,42] which is mainly attributed to the ultralow friction of our


DOI: 10.1021/acsnano.8b04654
ACS Nano XXXX, XXX, XXX−XXX

proposed design. In order to verify the low-friction property of this hybrid NG, the interaction force between the blade and the electrode is measured by the experimental setup shown in Supplementary Figure 7. Supplementary Figure 8 indicates that the interaction force is about 0.1 N when the rotation speed is 1200 rpm Therefore, the friction force between the Kapton blade and the Cu electrode can be calculated as 0.033 N, which is really a very low friction force. The detailed experiments and calculation are given in Supplementary Note 1.

In the current device, apart from the friction force between the blades and the electrodes, another force that hinders the rotation of the rotator mainly comes from the handmade electric brush in the EMG. In the near future, we will propose another EMG structure in which the coil is on the stator and the magnet is on the rotator. In this way, the electric brush will no longer be used in the EMG. Accordingly, the resistance force that hinders the rotation can be decreased greatly. As a result, the force that drives the hybrid NG to work will decrease to a large degree. Therefore, the hybrid NG without an electric brush can harvest rotation energy with a lower rotation speed and also can be used to detect lower wind speeds (<3.5m/s) or flow speeds. The related work is ongoing.

## CONCLUSIONS

An ultra-low-friction triboelectric−electromagnetic hybrid NG for harvesting rotation energy is presented in this paper. In this hybrid NG, the friction force is very small (at the level of 0.03 N) when the flexible and elastic polymer blades slide on the metal surface, since the contact between two triboelectric materials is very soft rather than rigid, as in traditional rotary TENGs. The optimization results show that the TENG made of a 4.5 cm × 4 cm × 25.4 $\mu$m FEP thin film has a higher output than other polymer films. Meanwhile, the open-circuit voltage of the TENG increases with the rotation speed, which is obviously different than a traditional rotary TENG. This was explained by the theory about the flexible cantilever and the centripetal force. The experimental results indicate the maximal load voltage and maximal load power per unit mass of the TENG and that of the EMG are 65 V and 438.9 mW/kg and 7 V and 181 mW/kg, respectively. It can be seen from the demonstration that this hybrid NG successfully powered a humidity/temperature sensor by harvesting weak wind energy. Meanwhile, the TENG can be used as a self-powered wind speed sensor. This ultra-low-friction hybrid NG will have great advantages and potential applications in scavenging weak rotation energy and weak wind energy and detecting the speed of weak wind.

## EXPERIMENTAL SECTION

**Fabrication of the Hybrid NG.** This hybrid NG mainly includes a rotator and a stator. The rotator is made of two cross-shaped acrylic plates and four rectangular acrylic plates. These acrylic plates are made by a laser cutter (PLS 6.75, Universal Laser Systems), and its thickness is 1.5 mm. When the rotator is rotating, it is like a cylinder with a radius of 2.5 cm and height of 4 cm. Then four groups of Cu coils are twined by us, and each coil has 100 turns. After that, four pieces of polymer thin films are cut into the designed dimensions and then attached on the sidewall of the rotator by glue. For the stator, the cylindrical frame is from a commercial electromagnetic motor. Eight pieces of Cu foil are attached evenly on the surface of the magnet. Finally, a shaft, which goes through the rotator, is connected to two gears on the top and bottom covers of the cylindrical stator frame. A handmade electric brush is assembled on the shaft and is used to connect the coil with the external circuit. A wind cup is fixed on the shaft; as a result, the rotator will rotate under the driving of external force. The mass of the TENG's materials and that of the EMG's materials are 1.18 g and 1.08 kg, respectively.

**Measurement of the Hybrid NG.** The output electrical perfromance of the hybrid NG was measured by an electrometer (Keithley, 6514) and a low-noise current preamplifier (Stanford Research System SR570). The data acquisition and analysis were performed by a LABVIEW platform and a data collector (NI USB 6211).

## ASSOCIATED CONTENT

### Supporting Information

The Supporting Information is available free of charge on the ACS Publications website at DOI: 10.1021/acsnano.8b04654.

Figures S1−S8 and Note 1 (PDF)

Movie S1: The hybrid NG harvesting rotation energy (AVI)

Movie S2: The hybrid NG harvesting wind energy and powering a small electric device (AVI)

## AUTHOR INFORMATION


### Corresponding Author

*E-mail: zhong.wang@mse.gatech.edu (Z. L. Wang).

### ORCID

Peihong Wang: 0000-0001-6386-8446

Lun Pan: 0000-0002-3083-4693

Zhong Lin Wang: 0000-0002-5530-0380


### Author Contributions

⊥P. Wang and L. Pan contributed equally to this work.

### Notes

The authors declare no competing financial interest.

## ACKNOWLEDGMENTS

This research was supported by the National Natural Science Foundation of China (61671017), Excellent Youth Talent Support Program in Colleges and Universities of Anhui Province in China (gxyqZD2018004), the China Scholarship Council, and the Hightower Chair Foundation of Georgia Institute of Technology of the USA.

## REFERENCES


(1) Iannacci, J. Internet of things (IoT); Internet of Everything (IoE); Tactile Internet; 5G-A (not so Evanescent) Unifying Vision Empowered by EH-MEMS (Energy Harvesting MEMS) and RF-MEMS (Radio Frequency MEMS). *Sens. Actuators, A* **2018**, *272*, 187−198.

(2) Khan, I.; Belqasmi, F.; Glitho, R.; Crespi, N.; Morrow, M.; Polakos, P. Wireless Sensor Network Virtualization: a Survey. *IEEE Commun. Surv. Tutorials* **2016**, *18*, 553−576.

(3) Wang, F.; Hu, L.; Hu, J.; Zhou, J.; Zhao, K. Recent Advances in the Internet of Things: Multiple Perspectives. *IETE Technol. Rev.* **2017**, *34*, 122−132.

(4) Wang, S.; Xu, J.; Wang, W.; Wang, G.-J. N.; Rastak, R.; Molina-Lopez, F.; Chung, J. W.; Niu, S.; Feig, V. R.; Lopez, J.; Lei, T.; Kwon, S.-K.; Kim, Y.; Foudeh, A. M.; Ehrlich, A.; Gasperini, A.; Yun, Y.; Murmann, B.; Tok, J. B.-H.; Bao, Z. Skin Electronics from Scalable Fabrication of an Intrinsically Stretchable Transistor Array. *Nature* **2018**, *555*, 83−88.

(5) Wang, J.; Li, S. M.; Yi, F.; Zi, Y. L.; Lin, J.; Wang, X. F.; Xu, Y. L.; Wang, Z. L. Sustainably Powering Wearable Electronics Solely by Biomechanical Energy. *Nat. Commun.* **2016**, *7*, 12744.

(6) Saliba, M. Perovskite Solar Cells Must Come of Age. *Science* **2018**, *359*, 388−389.




DOI: 10.1021/acsnano.8b04654
*ACS Nano* XXXX, XXX, XXX−XXX

(7) Tao, K.; Tang, L.; Wu, J.; Lye, S. W.; Chang, H. L.; Miao, J. M. Investigation of Multimodal Electret-based MEMS Energy Harvester with Impact-Induced Nonlinearity. *J. Microelectromech. Syst.* **2018**, *27*, 276−288.
(8) Wang, P.; Du, H. J. ZnO Thin Film Piezoelectric MEMS Vibration Energy Harvesters with Two Piezoelectric Elements for Higher Output Performance. *Rev. Sci. Instrum.* **2015**, *86*, 1131−1134.
(9) Halim, M.; Rantz, R.; Zhang, Q.; Gu, L.; Yang, K.; Roundy, S. An Electromagnetic Rotational Energy Harvester Using Sprung Eccentric Totor. *Appl. Energy* **2018**, *217*, 66−74.
(10) Wang, P.; Tanaka, K.; Sugiyama, S.; Dai, X.; Zhao, X.; Liu, J. A Micro Electromagnetic Low Level Vibration Energy Harvester Based on MEMS Technology. *Microsyst. Technol.* **2009**, *15*, 941−945.
(11) Fan, F. R.; Tian, Z. Q.; Wang, Z. L. Flexible Triboelectric Generator. *Nano Energy* **2012**, *1*, 328−334.
(12) Wang, Z. L. Triboelectric Nanogenerators as New Energy Technology and Self-Powered Sensors - Principles, Problems and Perspectives. *Faraday Discuss.* **2014**, *176*, 447−458.
(13) Wang, Z. L. On Maxwell's Displacement Current for Energy and Sensors: the Origin of Nanogenerators. *Mater. Today* **2017**, *20*, 74−82.
(14) Xu, C.; Zi, Y.; Wang, A. C.; Zou, H.; Dai, Y.; He, X.; Wang, P.; Wang, Y. C.; Feng, P.; Li, D.; Wang, Z. L. On the Electron-Transfer Mechanism in the Contact-Electrification Effect. *Adv. Mater.* **2018**, *30*, 1706790.
(15) Xu, M.; Wang, P.; Wang, Y. C.; Zhang, S. L.; Wang, A. C.; Zhang, C.; Wang, Z.; Pan, X.; Wang, Z. L. A Soft and Robust Spring Based Triboelectric Nanogenerator for Harvesting Arbitrary Directional Vibration Energy and Self-Powered Vibration Sensing. *Adv. Energy Mater.* **2018**, *8*, 1702432.
(16) Gao, S.; Wang, M.; Chen, Y.; Tian, M.; Zhu, Y.; Wei, X.; Jiang, T. An Advanced Electro-Fenton Degradation System with Triboelectric Nanogenerator as Electric Supply and Biomass-Derived Carbon Materials as Cathode Catalyst. *Nano Energy* **2018**, *45*, 21−27.
(17) Zhu, G.; Chen, J.; Zhang, T.; Jing, Q.; Wang, Z. L. Radial-Arrayed Rotary Electrification for High Performance Triboelectric Generator. *Nat. Commun.* **2014**, *5*, 3426.
(18) Wang, X.; Wang, S.; Yang, Y.; Wang, Z. L. Hybridized Electromagnetic-Triboelectric Nanogenerator for Scavenging Air-Flow Energy to Sustainably Power Temperature Sensors. *ACS Nano* **2015**, *9*, 4553−4562.
(19) Gao, S.; Chen, Y.; Su, J.; Wang, M.; Wei, X.; Jiang, T.; Wang, Z. L. Triboelectric-Nanogenerator-Powered Electrochemical Degradation of Organic Pollutant Using Pt-Free Carbon Materials. *ACS Nano* **2017**, *11*, 3965−3972.
(20) Xu, M.; Wang, Y. C.; Zhang, S. L.; Ding, W.; Cheng, J.; He, X.; Zhang, P.; Wang, Z.; Pan, X.; Wang, Z. L. An Aeroelastic Flutter Based Triboelectric Nanogenerator as a Self-Powered Active Wind Speed Sensor in Harsh Environment. *Extreme Mech. Lett.* **2017**, *15*, 122−129.
(21) Liu, R.; Kuang, X.; Deng, J.; Wang, Y. C.; Wang, A. C.; Ding, W.; Lai, Y. C.; Chen, J.; Wang, P.; Lin, Z.; Qi, H. J.; Sun, B.; Wang, Z. L. Shape Memory Polymers for Body Motion Energy Harvesting and Self-Powered Mechanosensing. *Adv. Mater.* **2018**, *30*, 1705195.
(22) Gao, S.; Su, J.; Wei, X.; Wang, M.; Tian, M.; Jiang, T.; Wang, Z. L. Self-Powered Electrochemical Oxidation of 4-Aminoazobenzene Driven by a Triboelectric Nanogenerator. *ACS Nano* **2017**, *11*, 770−778.
(23) Wang, X.; Wang, Z. L.; Yang, Y. Hybridized Nanogenerator for Simultaneously Scavenging Mechanical and Thermal Energies by Electromagnetic-Triboelectric-Thermoelectric Effects. *Nano Energy* **2016**, *26*, 164−171.
(24) Zhang, S. L.; Xu, M.; Zhang, C.; Wang, Y. C.; Zou, H.; He, X.; Wang, Z.; Wang, Z. L. Rationally Designed Sea Snake Structure Based Triboelectric Nanogenerators for Effectively and Efficiently Harvesting Ocean Wave Energy with Minimized Water Screening Effect. *Nano Energy* **2018**, *48*, 421−429.
(25) Wang, Z. L.; Jiang, T.; Xu, L. Toward the Blue Energy Dream by Triboelectric Nanogenerator Networks. *Nano Energy* **2017**, *39*, 9−23.
(26) Pan, L.; Wang, J.; Wang, P.; Gao, R.; Wang, Y. C.; Zhang, X.; Zou, J. J.; Wang, Z. L. Liquid-FEP-based U-Tube Triboelectric Nanogenerator for Harvesting Water-Wave Energy. *Nano Res.* **2018**, *11*, 4062−4073.
(27) Zi, Y.; Guo, H.; Wen, Z.; Yeh, M.; Hu, C.; Wang, Z. L. Harvesting Low-Frequency (< 5 Hertz) Irregular Mechanical Energy: A Possible Killer-Application of Triboelectric Nanogenerator. *ACS Nano* **2016**, *10*, 4797−4805.
(28) Wang, P.; Liu, R.; Ding, W.; Zhang, P.; Pan, L.; Dai, G.; Zou, H.; Dong, K.; Xu, C.; Wang, Z. L. Complementary Electromagnetic-Triboelectric Active Sensor for Detecting Multiple Mechanical Triggering. *Adv. Funct. Mater.* **2018**, *28*, 1705808.
(29) Zhang, C.; Tang, W.; Han, C. B.; Fan, F. R.; Wang, Z. L. Theoretical Comparison, Equivalent Transformation, and Cconjunction Operations of Electromagnetic Induction Generator and Triboelectric Nanogenerator for Harvesting Mechanical Energy. *Adv. Mater.* **2014**, *26*, 3580−3591.
(30) Zhong, X.; Yang, Y.; Wang, X.; Wang, Z. L. Rotating-Disk-Based Hybridized Electromagnetic-Triboelectric Nanogenerator for Scavenging Biomechanical Energy as a Mobile Power Source. *Nano Energy* **2015**, *13*, 771−780.
(31) Guo, H.; Wen, Z.; Zi, Y.; Yeh, M.; Wang, J.; Zhu, L.; Hu, C.; Wang, Z. L. A Water-Proof Triboelectric-Electromagnetic Hybrid Generator for Energy Harvesting in Harsh Environments. *Adv. Energy Mater.* **2016**, *6*, 1501593.
(32) Wen, Z.; Guo, H.; Zi, Y.; Yeh, M.; Wang, X.; Deng, J.; Wang, J.; Li, S.; Hu, C.; Zhu, L.; Wang, Z. L. Harvesting Broad Frequency Band Blue Energy by a Triboelectric-Electromagnetic Hybrid Nanogenerator. *ACS Nano* **2016**, *10*, 6526−6534.
(33) Xie, Y.; Wang, S.; Niu, S.; Lin, L.; Jing, Q.; Su, Y.; Wu, Z.; Wang, Z. L. Multi-Layered Disk Triboelectric Nanogenerator for Harvesting Hydropower. *Nano Energy* **2014**, *6*, 129−136.
(34) Zhang, H.; Yang, Y.; Zhong, X.; Su, Y.; Zhou, Y.; Hu, C.; Wang, Z. L. Single-Electrode-Based Rotating Triboelectric Nanogenerator for Harvesting Energy from Tires. *ACS Nano* **2014**, *8*, 680−689.
(35) Tang, W.; Zhang, C.; Han, C.; Wang, Z. L. Enhancing Output Power of Cylindrical Triboelectric Nanogenerators by Segmentation Design and Multilayer Integration. *Adv. Funct. Mater.* **2014**, *24*, 6684−6690.
(36) Bai, P.; Zhu, G.; Liu, Y.; Chen, J.; Jing, Q.; Yang, W.; Ma, J.; Zhang, G.; Wang, Z. L. Cylindrical Rotating Triboelectric Nanogenerator. *ACS Nano* **2013**, *7*, 6363−6366.
(37) Wang, S.; Xie, Y.; Niu, S.; Lin, L.; Wang, Z. L. Freestanding Triboelectric-Layer-Based Nanogenerators for Harvesting Energy from a Moving Object or Human Motion in Contact and Non-Contact Modes. *Adv. Mater.* **2014**, *26*, 2818−2824.
(38) Niu, S.; Liu, Y.; Chen, X.; Wang, S.; Zhou, Y. S.; Lin, L.; Xie, Y.; Wang, Z. L. Theory of Freestanding Triboelectric-Layer-Based Nanogenerators. *Nano Energy* **2015**, *12*, 760−774.
(39) Wang, J.; Ding, W.; Pan, L.; Wu, C.; Yu, H.; Yang, L.; Liao, R.; Wang, Z. L. Self-Powered Wind Sensor System for Detecting Wind Speed and Direction Based on a Triboelectric Nanogenerator. *ACS Nano* **2018**, *12*, 3954−3963.
(40) Kovacs, G. T. A. *Micromachined Transducers Sourcebook* (Simplified Chinese ed.); McGraw-Hill: New York, 1998; pp 135−136.
(41) Xi, Y.; Guo, H.; Zi, Y.; Li, X.; Wang, J.; Deng, J.; Li, S.; Hu, C.; Cao, X.; Wang, Z. L. Multifunctional TENG for Blue Energy Scavenging and Self-Powered Wind-Speed Sensor. *Adv. Energy Mater.* **2017**, *7*, 1602397.
(42) Quan, Z.; Han, C. B.; Jiang, T.; Wang, Z. L. Robust Thin Films-Based Triboelectric Nanogenerator Arrays for Harvesting Bidirectional Wind Energy. *Adv. Energy Mater.* **2016**, *6*, 1501799.


DOI: 10.1021/acsnano.8b04654
*ACS Nano* XXXX, XXX, XXX−XXX